한국해양공학회지 제15권 제2호, pp 11~21, 2001 (ISSN 1225-0767)

Performance of the Submerged Dual Buoy/Membrane Breakwaters in Oblique Seas

S. T. KEE

Dept. of Civil Eng., Seoul National University of Technology, Seoul, Korea

KEY WORDS: flexible membrane, submerged and floating breakwater, wave-flexible structure interaction, boundary element method

ABSTRACT: *The focus of this paper is on the numerical investigation of obliquely incident wave interactions with a system composed of fully submerged and floating dual buoy/vertical-flexible-membrane breakwaters placed in parallel with spacing between two systems. The fully submerged two systems allow surface and bottom gaps to enable wave transmission over and under the system. The problem is formulated based on the two-dimensional multi-domain hydro-elastic linear wave-body interaction theory. The hydrodynamic interaction of oblique incident waves with the combination of the rigid and flexible bodies was solved by the distribution of the simple sources (modified Bessel function of the second kind) that satisfy the Helmholz governing equation in fluid domains. A boundary element program for three fluid domains based on a discrete membrane dynamic model and simple source distribution method is developed. Using this developed computer program, the performance of various dual systems varying buoy radiuses and drafts, membrane lengths, gaps, spacing, mooring-lines stiffness, mooring types, water depth, and wave characteristics is thoroughly examined. It is found that the fully submerged and floating dual buoy/membrane breakwaters can, if it is properly tuned to the coming waves, have good performances in reflecting the obliquely incident waves over a wide range of wave frequency and headings.*

INTRODUCTION

The advantages of floating flexible membrane wave barriers over conventional fixed breakwaters include their reduced environmental impacts, ability of relocation, simple sacrificial design, free from bottom foundation consideration, and comparably low cost in deep water constructions. Membrane systems have been proposed for use as portable temporary breakwaters, submerged breakwaters, contaminant booms for floating oil slicks, silt curtains, and for storage and transportation of fluid in the ocean (Amal C *et al.*, 2001). A number of vertical floating flexible membrane breakwaters have been investigated by Thompson *et al.* (1992), Aoki et al. (1994), Kim and Kee (1996, 1997), Williams (1996). Kim and Kee (1996, 1997) developed an analytical model for wave transmission and reflection by a vertical pre-tensioned membrane using the eigenfunction expansion method and also presented a numerical solution of the problem employing simple source distribution method. Their results showed that the a good performance can be obtained in spite of appreciable sinusoidal motions of membrane because the vertical sinusoidal motions tends to generate only exponentially decaying local (evanescent) wave in the lee side. These methods were latter applied to dual vertical floating flexible membrane system (Cho *et al.*, 1997; 1998) in oblique seas, and a horizontal membrane and verified by laboratory experiments (Cho and Kim, 1998; 2000).

In practice, a fairly good performance as breakwaters in wide frequency region including long waves, a major fraction of the water column needs to be occupied by the system. In view of this, the vertical flexible membrane system was composed of surface pierced buoys and vertical flexible membranes hinged at seafloor. However, these breakwaters expect large wave loadings and possible blockage of aesthetic view, water circulation, sediment transport, fish passage, and surface vessel passing.

In the present paper, fully submerged vertical flexible membrane breakwaters with gaps between bottom of system and seafloor are adopted for their performance investigation in oblique seas. One reason of the adoption of the fully submerged breakwaters with bottom gaps is that such breakwaters are favored from the point of view of a marine scenario. Another significant reason is that free exchange of water mass and sediment through the gaps supplied by the system. So the water in the sheltered region can be kept circulating and therefore prevent stagnation and pollution. And the seabed profiles can be kept in general partitioning the natural sea.

For the analysis of these submerged floating breakwater system, we assumed that buoy and membrane motions are uniform in the longitudinal direction and small to allow linear theory. It is also assumed, for simplicity, that buoy is rigid and the heave motion of buoy is negligible due to large initial tension. The coupling of buoy and membrane motions was taken into consideration through an appropriate boundary condition at the joint. The velocity potentials

of wave motion are fully coupled with membrane deformation. The membrane motion and the rigid body motion of a buoy become dynamically coupled with each other, thus the membrane motion and velocity potentials need to be solved simultaneously. Numerical results are presented to check the accuracy and validity of the present multi-domains boundary element program by the energy-conservation formula and convergence test. The present study deal with the fully submerged floating buoy/membrane subject to oblique incident wave and focuses on the resonance and response characteristics, which are important in the design and operation of the system, but have not been adequately studied before.

THEORY AND NUMERICAL METHOD

With a reference to Fig. 1, the oblique incident wave and buoy/membrane interaction problem in multi-fluid domain and with the geometry are defined with a Cartesian coordinate system x-y, in which x is measured horizontally, and y is measured vertically upward from the still water level. The system is idealized as two-dimensional allowing that wave and system motions are uniform in z direction. The system is subjected to an incident train of regular, monochromatic, small amplitude A, harmonic motion of frequency ω, obliquely propagating with an angle θ $(0<\theta<\pi/2)$ to x-axis in water of arbitrary depth h as depicted in Fig. 1. The ideal flow field can be described in terms of the time-harmonic total velocity potential for an oblique incident wave:

$$\Phi(x,y,z,t)=Re[\{\phi_o(x,y)+\phi(x,y)e^{ik_z z-i\omega t}] \tag{1}$$

$$\phi_o=\frac{igA}{\omega}\frac{\cosh k_o(y+h)}{\cosh k_o h}e^{ik_o\cos\theta x} \tag{2}$$

where $i=\sqrt{-1}$, t denotes time, $k_z=k_o\sin\theta$ is the wave number k_o component in the z direction, and is related to the angular frequency through the dispersion relation $\omega^2=k_o g\tanh k_o h$ with g being the gravitational acceleration. ϕ_o is the known incident potential and ϕ is the time-independent unknown scattered potential, which includes both diffraction and radiation effects.

The unknown scattered complex velocity potentials, ϕ_1, ϕ_2 and ϕ_3, in three fluid domains I, II and III (see Fig. 1.) satisfy the Helmholtz equation $\nabla^2\phi_l-k_z^2\phi_l=0$, $(l=1,2,3)$ as governing equation and the following linearized free-surface (Γ_F), bottom (Γ_b), and radiation conditions(Γ_C):

$$\frac{\partial\phi_l}{\partial y}=\frac{\omega^2}{g}\phi_l \quad (on\ \Gamma_F) \tag{3}$$

$$\frac{\partial\phi_l}{\partial y}=0 \quad (on\ \Gamma_b) \tag{4}$$

$$\lim_{|x|\to\infty}\left(\frac{\partial}{\partial x}\pm ik_x\right)\begin{pmatrix}\phi_1\\ \phi_3\end{pmatrix}=0 \quad (on\ \Gamma_c) \tag{5}$$

where Γ_C is the vertical truncation boundaries at far fields and $n=(n_x,n_y)$ is the unit outward normal vector. In the numerical implementation, the radiation boundary condition is applied on Γ_C located at a finite distance from the edge of structures. Under large initial tension, we assume, for simplicity, that the heave motions of the buoys are negligible. Then the boundary condition on the floating buoys in each fluid domain is

$$\frac{\partial\phi_l}{\partial n}+i\omega\{\eta_1 n_x+\eta_3 n_\theta\}+\frac{\partial\phi_o}{\partial n}=0, \quad l=1,2,3 \tag{6}$$

where $n_\theta=xn_y-yn_x$, and the symbols η_1, η_3 represent complex sway and roll responses of buoys respectively. In addition, the scattered unknown potentials must satisfy the following linearized kinematic/dynamic boundary conditions on the membrane surface:

$$\frac{\partial\phi_l}{\partial x}=-\frac{\partial\phi_{l+1}}{\partial x}=-i\omega\xi \tag{7}$$

$$\frac{d^2\xi}{dy^2}+\lambda^2\xi=\frac{\rho i\omega}{T}(\phi_i-\phi_{i+1}) \quad (on\ \Gamma_m) \tag{8}$$

where ρ is the fluid density, $\lambda=\omega\sqrt{m/T}$ with T and m being the membrane tension and mass per unit length for front membrane system, respectively. The harmonic membrane motions are $\Xi(y,t)=Re[\xi(y)e^{ik_z z-i\omega t}]$. In addition, the surface and bottom gaps must satisfy the following vertical fictitious boundary condition(Γ_f) based on the continuity of hydrodynamic pressure and normal fluid velocity.

$$\phi_l=\phi_{l+1}, \quad \frac{\partial\phi_l}{\partial x}=-\frac{\partial\phi_{l+1}}{\partial x} \quad at\ \Gamma_f \tag{9}$$

Since buoys are connected to the membranes, the coupled dynamic equations need to be solved. Unlike rigid body hydrodynamics, the body boundary condition on membrane is not known in advance. Therefore, the membrane and buoy motions and velocity potentials need to be solved simultaneously. To solve the present boundary value problem, a three-domain boundary integral equation method using simple sources along the entire boundary is developed. Using Green's second identity, the unknown scattered potential can be expressed as

$$C\phi_l(x,y)=\int_\Gamma\left\{\phi_l(x',y')\frac{\partial G}{\partial n}-G(x,y,x',y')\frac{\partial\phi_l}{\partial n}\right\}d\Gamma \tag{10}$$

where C=solid-angle constant and the integral covers the entire boundary of each fluid region, (x,y) and (x',y') are field point and source point, respectively. The fundamental solution (Green function) of the Helmholtz equation and its the normal derivative of G are given by

$$G=-\frac{1}{2\pi}K_o(k_z r) \tag{11}$$

$$\frac{\partial G}{\partial n}=\frac{1}{2\pi}k_z K_1(k_z r)\frac{\partial r}{\partial n} \tag{12}$$

When the source point shrinks to the field point on boundary i.e., when $r \to 0$ a singularity exists due to the presence of $K_o(\lambda r)$, and the analytic solution for this integration is impossible. One can use the following existing approximations in the Cauchy principal value sense.

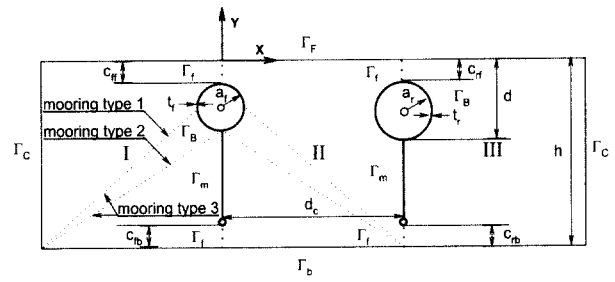

Fig. 1 Coordinate system and integration domains for dual fully submerged buoy/membrane breakwater

$$\int_\Gamma \lambda K_1(\lambda r)\frac{\partial r}{\partial n}\,d\Gamma = 0 \tag{13}$$

$$\int_\Gamma \lambda K_o(\lambda r)d\Gamma = \int_\Gamma -\gamma - \ln\left(\frac{\lambda r}{2}\right)d\Gamma$$

$$= \int_\Gamma -\gamma + \ln\left(\frac{\lambda}{2}\right)\ln\left(\frac{1}{r}\right)d\Gamma \tag{14}$$

Applying Green's second identity in each of the domains to the unknown potentials ϕ_l and imposing the relevant boundary conditions, the integral equations in each fluid domain can be written as

$$C\varphi_l = \frac{1}{2\pi}\int_\Gamma \left\{k_z K_1(k_z r)\frac{\partial r}{\partial n}\varphi_l + K_o(k_z r)\frac{\partial \varphi_l}{\partial n}\right\}d\Gamma \tag{15}$$

In Eq. (15), all the boundary conditions of ϕ_l except for the dynamic boundary conditions of buoy and membrane can be straightforwardly implemented.

Imposing the boundary conditions, Eqs. (3)~(7) into Eq. (15), the integral equations in each fluid domain can be written as

$$C\phi_l + \int_{\Gamma_l}[k_z K_1(k_z r)\frac{\partial r}{\partial n} - \nu K_o(k_z r)]\phi_l d\Gamma$$

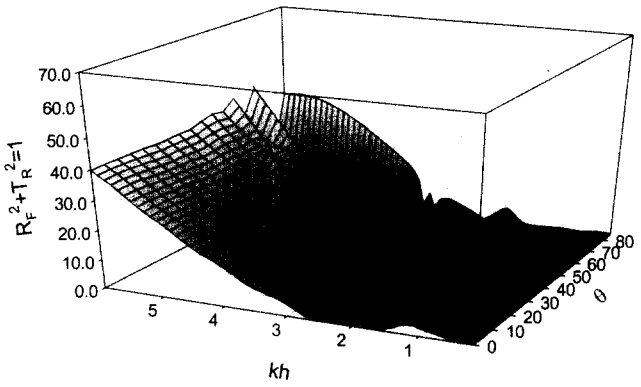

Fig. 2a Convergence test of BEM(N=100) for $T_i/K_{ij}=0.1$, $t_i/a_i=0.02$, $a_f/h=0.125$, $a_r/h=0.2$, $c_{ik}/h=0.125$, $d_c/h=1$

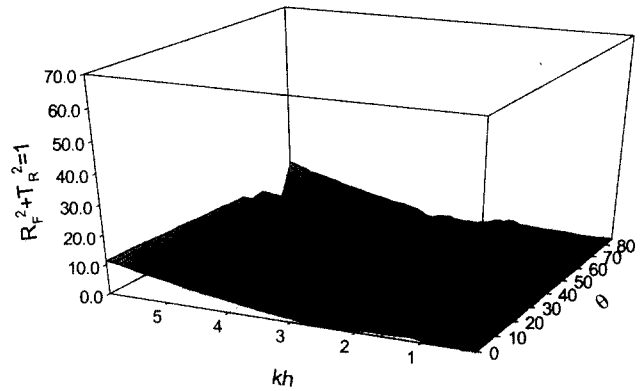

Fig. 2b Convergence test of BEM(N=200) for $T_i/K_{ij}=0.1$, $t_i/a_i=0.02$, $a_f/h=0.125$, $a_r/h=0.2$, $c_{ik}/h=0.125$, $d_c/h=1$

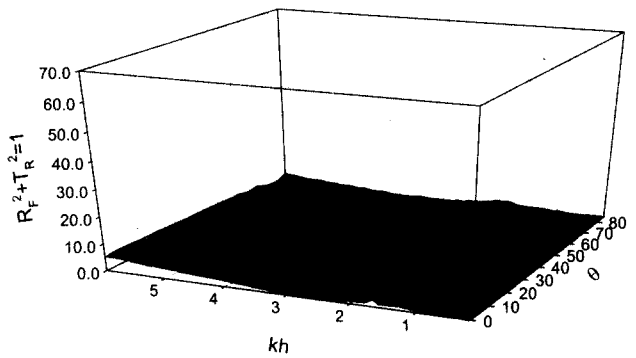

Fig. 2c Convergence test of BEM(N=280) for $T_i/K_{ij}=0.1$, $t_i/a_i=0.02$, $a_f/h=0.125$, $a_r/h=0.2$, $c_{ik}/h=0.125$, $d_c/h=1$

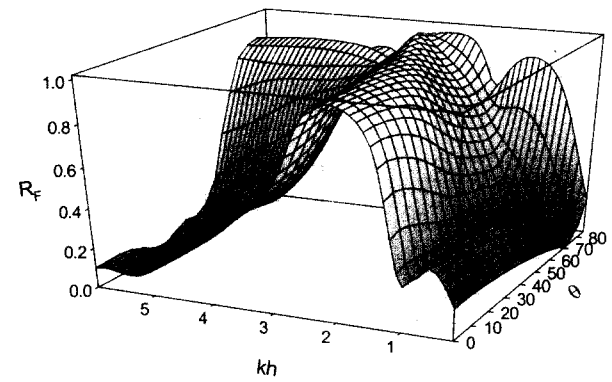

Fig. 2d The reflection coefficient as function kh and θ for $T_i/K_{ij}=0.1$, $t_i/a_i=0.02$, $a_f/h=0.125$, $a_r/h=0.2$, $c_{ik}/h=0.125$, $d_c/h=1$

$$+\int_{\Gamma_C}[k_zK_1(k_zr)\frac{\partial r}{\partial n}-ik_xK_o(k_zr)]\phi_l d\Gamma$$
$$+\int_{\Gamma_b}\phi_l k_zK_1(k_zr)\frac{\partial r}{\partial n}\,d\Gamma$$
$$+\int_{\Gamma_m}[\phi_l k_zK_1(k_zr)\frac{\partial r}{\partial n}s_l(i\omega\xi)K_o(k_zr)]d\Gamma$$
$$+\int_{\Gamma_B}[\phi_l k_zK_1(k_zr)\frac{\partial r}{\partial n}$$
$$+i\omega K_o(k_zr)(\eta_1 n_x+\eta_3 n_\theta)+K_o(k_zr)\frac{\partial\phi_o}{\partial n}]d\Gamma=0$$
$$(l=1,2,3) \tag{16}$$

where $\nu=\omega^2/g$ is the infinite-depth wave number. C is solid angle constant, and ($s_1=1$, $s_2=-1$) for fluid domains I, II and ($s_2=1$, $s_3=-1$) for fluid domains II, III, since the front and rear membrane and buoy have two fluid domains (I, II) and (II, III) respectively as depicted in Fig.1. The integration of open boundary has to be vanished in Domain II.

To solve Eq. (16), the entire boundary is discretized into a large finite number of segments. On each segment the potential is assumed to be constant, and the singularities G and $\partial G/\partial n$ are integrated analytically in Eqs. (13)~(14). The integral Eq. (16) can then be transformed to the corresponding algebraic matrix equation. For instance, if each of half fluid domain is discretized by $N=N_F+N_C+N_b+N_m+N_B+N_f$ segments, there are $3N$ unknowns for ϕ_1, ϕ_2 and ϕ_3, $2N_m$ unknowns for displacements ξ of dual membranes, and four more unknowns two η_1 and η_3 for two buoys. Therefore, $3N+2N_m+4$ linear simultaneous equation has to be solved. Eq. (16) cannot be, however, solved for ϕ_l independently since ξ and η_1, η_3 are unknown. The Eq. (16) should be coupled with the equations of motion of the membranes and buoys.

The discrete form of the equation of membrane motion for $j-th$ element is given by

$$\rho i\omega(\phi_{i(j)}-\phi_{i+1(j)})l_j-T_{(j)}\left(\frac{\partial\xi_f}{\partial\zeta}\right)_j+T_{(j+1)}\left(\frac{\partial\xi_f}{\partial\zeta}\right)_{j+1}$$
$$=-ml_j\omega^2\xi_{(j)} \tag{17}$$

where $\left(\frac{\partial\xi_f}{\partial\zeta}\right)_j=(\xi_{f(j)}-\xi_{f(j-1)})/\triangle\zeta_j$

The symbol l_j is the length of the $j-th$ segment, and $\triangle\zeta_j=(l_j+l_{j+1})/2$. The geometric boundary conditions at the seabed and the top connection points of membrane $(0,-d_c)$ are

$$\xi=0 \text{ at } y=-h,\quad \xi=\eta_1+R\eta_3 \text{ at } y=-d_c \tag{18}$$

where R is the distance from the connection point $(0,-d_c)$ to rotation center of buoy. The Eq. (17) can in principle be solved for variable tensions. In the present study, however, we assume that the initial tension T is much greater than membrane weight or dynamic tension thus can be regarded as constant.

Next, we consider the rigid-body motion of buoys. As mentioned before, it is assumed that the heave response is negligible due to large initial tension. The coupled equations of motion for sway and roll are given by

$$M(-\omega^2)X=F_p-(K_{HS}+K_m)X-F_T+F_D \tag{19}$$

where $X=[\eta_1\ \eta_3]^T$, and the mass matrix M are given by

$$M=\begin{bmatrix} m_o & -m_oy_c \\ -m_oy_c & I\end{bmatrix} \tag{20}$$

where m_o is the mass of the buoy, and y_c is the vertical coordinate of the center of mass, and I is the roll moment of inertia. The potential hydrodynamic forces and moments F_p can be calculated from the integration of hydrodynamic pressures over the buoy surface:

$$F_p=i\rho\omega\sum_{N_B}\begin{Bmatrix}(\phi_o+\phi_1)n_x\triangle l_j+(\phi_o+\phi_2)n_x\triangle l_j\\(\phi_o+\phi_1)n_\theta\triangle l_j+(\phi_o+\phi_2)n_\theta\triangle l_j\end{Bmatrix} \tag{21}$$

where $\triangle l_j$ is the length of each segment of the buoy surface. The restoring forces and moments due to the hydrostatic pressure are given by

$$K_{HS}=\begin{Bmatrix}0 & 0\\0 & \rho g\int_W x^2dx+\forall\rho gy_b-mgy_c\end{Bmatrix} \tag{22}$$

where $\forall$ is the displaced volume, and y_b is the vertical coordinate of the center of buoyancy for each buoy. For simplicity, we assume that the mooring lines are massless and symmetric with respect to the y axis. Taking the angles of mooring line with the horizontal (toe angles) as β, the attachment points on the cylinders as $(x_p,y_p)$and the two dimensional spring constants of the mooring lines as K, the resultant sway and roll mooring stiffness are given by (Patel, 1990)

$$K_m=2K\begin{bmatrix}\cos^2\beta & -S\cos\beta\\-S\cos\beta & S^2\end{bmatrix} \tag{23}$$

where $S=|x_p|\sin\beta-|y_p|\cos\beta$

At the connection points between membranes and buoys, the tensions cause the following forces and moments on the buoys:

$$F_T=T_{(N_m+1)}\begin{Bmatrix}-\sin\alpha\\R\sin\eta_3\cos\alpha-R\cos\eta_3\sin\alpha\end{Bmatrix} \tag{24}$$

where α is the angle of membrane at the connections with respect to the y axis for each buoy, and the symbol R is the radial

distances from the center of rotation of buoy to the connection points on each buoy. Assuming the angle α is small, $\cos\alpha \cong 1$, $\sin\alpha \cong -\left(\frac{\partial \xi}{\partial \zeta}\right)_{N_m+1}$, and Eq. (24) can be rewritten as

$$F_T = T_{(N_m+1)} \begin{bmatrix} \frac{2}{l_{N_m}} & \frac{2R}{l_{N_m}} \\ \frac{2R}{l_{N_m}} & R+\frac{2R^2}{l_{N_m}} \end{bmatrix} \begin{Bmatrix} \eta_1 \\ \eta_3 \end{Bmatrix} - T_{(N_m+1)} \begin{bmatrix} \frac{2}{l_{N_m}} \\ \frac{2R}{l_{N_m}} \end{bmatrix} \quad (25)$$

We can see that the first terms of Eq. (25) give positive restoring forces and moments to the each buoy, while the second terms act as sources of excitation proportional to the motion amplitude of the neighboring membrane element. Therefore, the membrane tensions can be either restoring forces or excitations. For the present numerical results, viscous drag forces F_D are not included unless mentioned otherwise, and these are detailed in Kee & Kim (1997).

NUMERICAL RESULTS AND DISCUSSIONS

The three-domain boundary element program developed as described in the preceding section was used to demonstrate the performance of fully submerged dual buoy/membrane wave barriers in oblique incident waves. As coordinate system and computational domain are defined in Fig. 1, the two submerged system in parallel with spacing d_c. Based on previous study (Kee & Kim, 1997) the efficiency for larger mooring stiffness is higher, and the best performance can be achieved for the dual mooring system (mooring type 3). The toe angles of mooring type 1 and 2 are 33° and 29.6°, respectively. The upper mooring line (type 1) is attached to the side of maximum width, while the lower mooring line (type 2) is attached at the bottom of the buoy. The submerged buoy/membrane system allows gaps $c_{ik}(i=f, r)\ (k=f, b) \rightarrow c_{ff}, c_{fb}, c_{rf}, c_{rb}$, which present front (f) free surface (f) gap, front (f) bottom (b) gap, rear (r) free surface (f) gap, rear (r) bottom (b) gap respectively.

The convergence test of the developed BEM program for the system design parameter $T_i/K_{ij}=0.1$, $t_i/a_i=0.02$, $a_f/h=0.125$, $a_r/h=0.2$, $c_{ik}/h=0.125$, $d_c/h=1$. $T_i(i=f, r)$ is tension of front (f) and rear (r) membrane. $K_{ij}(i-f, r), (j=1,2)$ is mooring stiffness, $j=1,2$denotes upper (1) and down (2) mooring lines. Figs. 2a~2c. show the results with increasing the number of segments N=100, 200, 280 in fluid domain I, and were checked against the error that was calculated from the energy conservation relation $R_F^2+T_R^2=1$. It is seen that the errors uniformly decrease in a domain of kh and θ as the number of segments is increased. From those tests, the number of total elements in the first fluid domain $N=280$ gave sufficient accuracy, and thus was used for the ensuing further computation. Fig. 2d. shows the results as function of non-dimensional frequency kh and incident wave angles θ. It is seen that almost complete refection in vicinity of $kh=2.3$, and for a wide of wave headings, however, allows wave transmission for other frequencies and wave headings.

When the system has a various spacing like $d_c/h=1,2,3$ for $c_{ik}/h=0.125$ and a smaller radius of rear buoy without mooring lines, the varying performances are shown in Figs. 3 a~3c. It is seen that the efficiency for increased spacing is not improved except the narrow band of the low frequency and high wave headings. We can expect a relatively good performance at high frequency band if the motions of buoy are allowed in fluid field. Since the scattered wave generated by motion of buoys has possible mutual cancellation effects against incident waves. Therefore the submerged system needs to be positioned close to the free surface to get higher disturbance in high wave energy region. So the free surface gaps are narrowly set as $c_{ff}=c_{rf}=0.05$, and its efficiency is shown in Fig. 4. Its performance in high frequency region is some what improved compared to that of deeper free surface gaps (Figs. 3a.).

When the large sizes of buoys $a_f/f=a_r/h=0.2$ are employed for systems with strong mooring stiffness $T_i/K_{ij}=0.1$, mooring type 3, $c_{ik}/h=0.125$, and $d_c/h=1$. The efficiency for this breakwater is shown in Fig 5. Except high incident wave angle $\theta=85^\circ$ the performance is generally poor enough to transmit most waves. Although strong mooring system can insure the vertical sinusoidal manner of membrane motion that transfer the incident wave to the exponentially decaying local standing wave, the hydrodynamic effects of membrane motions are not significantly influenced to near fluid field since the membrane occupied only partial part of water column. In addition the wave are hardly generated thanks to buoys restrained strongly by mooring lines. Therefore almost all waves are passing over and beneath systems without mutual cancellations with reflected and radiated waves.

After removing upper mooring line of rear buoy, only mooring lines at joint (mooring type 2) exist, and it allows motions similar to the pivoted vibration at joint. The dramatically enhanced performance over wide frequency range and wave headings is shown in Fig. 6. The scattered waves by the motion of rear buoy excite mutual cancellation against obliquely incident waves, scattered waves by motion of rear membrane and front buoy/membrane. In addition it shows insights of a physical

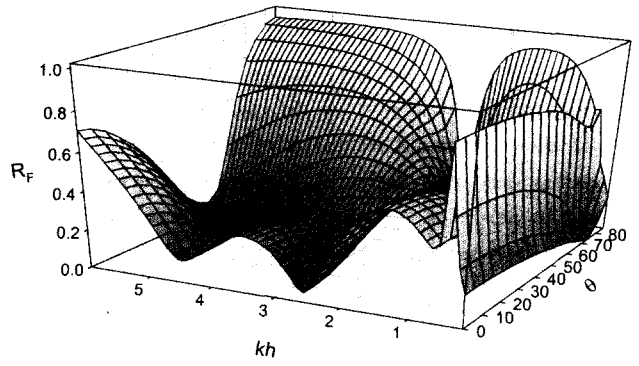

Fig. 3a The reflection coefficient as function kh and θ for $T_f/K_{fj}=0.1$, $T_r/K_{rj}=0$, $t_i/a_i=0.02$ $a_f/h=0.2$, $a_r/h=0.125$, $c_{ik}/h=0.125$, $d_c/h=1$

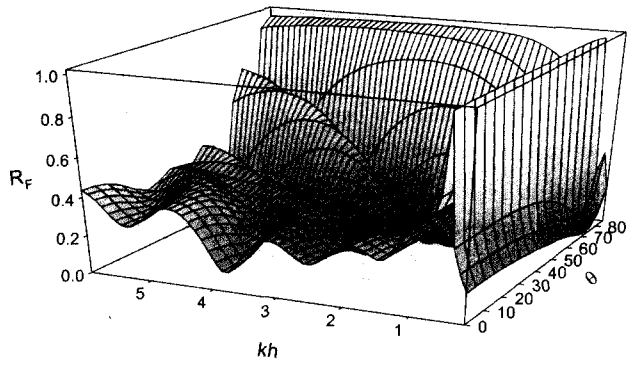

Fig. 3b The reflection coefficient as function kh and θ for $T_f/K_{fj}=0.1$, $T_r/K_{rj}=0$, $t_i/a_i=0.02$, $a_f/h=0.2$, $a_r/h=0.125$, $c_{ik}/h=0.125$, $d_c/h=2$

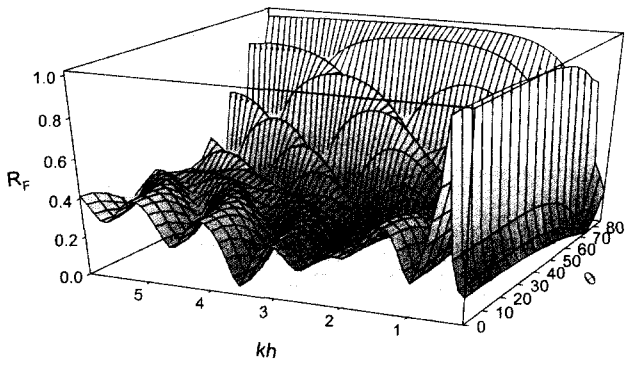

Fig. 3c The reflection coefficient as function kh and θ for $T_f/K_{fj}=0.1$, $T_r/K_{rj}=0$, $t_i/a_i=0.02$, $a_f/h=0.2$, $a_r/h=0.125$, $c_{ik}/h=0.125$, $d_c/h=3$

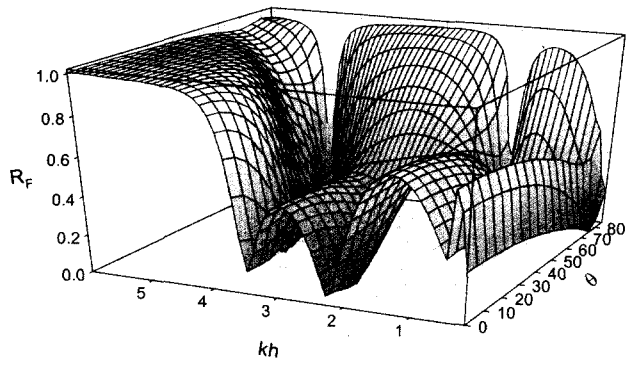

Fig. 4 The reflection coefficient as function kh and θ for $T_f/K_{fj}=0.1$, $T_r/K_{rj}=0$, $t_i/a_i=0.02$, $a_f/h=0.2$, $a_r/h=0.125$, $c_{ff}/h=0.05$, $c_{fb}/h=0.125$, $c_{rf}/h=0.05$, $c_{rb}/h=0.125$, $d_c/h=1$

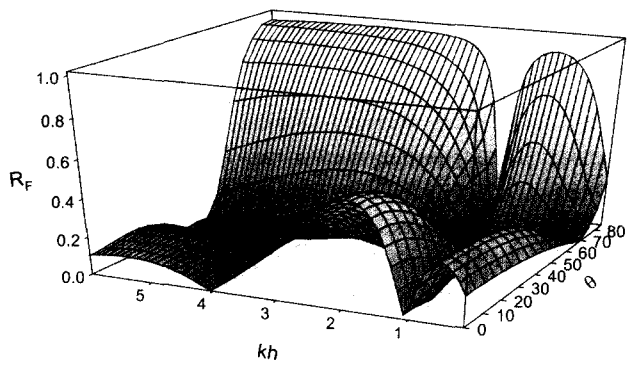

Fig. 5 The reflection coefficient as function kh and θ for $T_i/K_{ij}=0.1$, $t_i/a_i=0.02$, $a_i/h=0.2$, $c_{ik}/h=0.125$, $d_c/h=1$

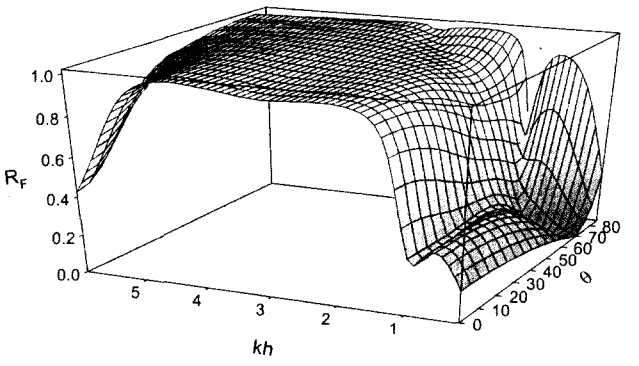

Fig. 6 The reflection coefficient as function kh and θ for $T_f/K_{fj}=0.1$, $T_r/K_{r1}=0$, $T_r/K_{r2}=0.1$, $t_i/a_i=0.02$, $a_i/h=0.2$, $c_{ik}/h=0.125$, $d_c/h=1$

phenomena magnifying the wave trapping effects between two systems. After takes off only upper mooring line (mooring type 1) of each buoy, those two systems have same design parameters. For this breakwater more severe scattered potential flow generated by motions of two buoys and membranes in fluid field. Fig. 7. shows the performance for $T_f/K_{f1}=0$, $T_f/K_{f2}=0.1$, $t_f/a_f=0.02$, $a_f/h=0.2$, $c_{fk}/h=0.125$, $d_c/h=1$ in which the resonance regions characterized by sharp drop in efficiency.

When all gap is narrow like $c_{fk}/h=0.05$ for $T_f/K_{f1}=0$, $T_f/K_{f2}=0.1$, $t_f/a_f=0.02$, $a_f/h=0.2$, $d_c/h=1$ almost complete reflections occur over wide frequency and incident wave angles except of narrow band of long wave frequency and resonance frequencies as shown in Fig.8. Resonance of system usually results, however, in failure of function or gives a damage of system integrity. Thus every designer seeks methods to remove such resonance in system. After tuning system to have asymmetric design parameters, simply changing of gaps in its geometry as $c_{ff}/h=0.125$, $c_{rf}/h=0.05$, $c_{fb}/h=0.05$ and $c_{rb}/h=0.125$, the resonance in Fig. 9. is slightly reduced when it compared to that in Fig. 7.

The wave load is exponentially decaying downward direction to water depth. Therefore the response of the submerged membrane system will be quite different with that of surface-piercing case. Since the rapid variation of the potential flow exists near the top ends of structures.

Three different dual membrane systems without buoys have been tested numerically: (case1) surface-piercing dual membrane extended to sea floor, (case2) submerged dual membrane with free-surface gaps, (case3) submerged dual membrane with free-surface/bottom gaps. In Figs.10a~10b, motions of front membrane at frequency $kh=0.2, 6.0$ is shown for three different system with non-dimensional membrane tension $\tilde{T}=0.255$, and $\tilde{T}$ is $(T/\rho g h^2)$. For $kh=0.2$ long wave region, motions of membranes are significantly changed according to types of gaps. The reflection coefficients for those three cases are $R_F=1.0, 0.36, 0.12$, respectively. However, at high frequency region $kh=6.0$ motions of submerged membrane are larger than those of $kh=0.2$, and reflection coefficients varies as $R_F=1.0, 0.06, 0.61$. It is seen that the performance in long waves is improved as the gaps decreased. When gap is small compared to wavelength, only local waves are generated by front membrane and excite the sinusoidal motion of the rear membrane.

Incident wave interaction with both submerged buoy/membranes is quite complicated. It generates radiated waves and re-reflected waves between two systems so that such scattered waves have phase differences among themselves. Adjusting these phase differences by gaps can make their wave amplitude offset themselves. Therefore, a simple large motion of membranes and buoys does not always aggravate its performance. Thus the motions of membrane and buoy have to be checked against sharp or a small kink resonance in its performance. Parameters of system tunings includes gaps, radius of buoys, mooring types, mooring stiffness, gaps, mass of buoy et al. In this study we found that most significant parameter is mooring type and radius of buoys for this dual submerged/floating system with surface/bottom gaps. The resonance of system is important for its design and application in the ocean environment. The one of well tuned up systems in this presentation is the system adjusted by its mooring types, and its efficiency is shown in Fig. 6.

Fig. 6 shows the performance for the dual submerged system without upper mooring line (mooring type 2) of rear buoys for $T_f/K_{ff}=0.1$, $T_r/K_{r1}=0$, $T_r/K_{r2}=0.1$, $a_f/h=a_r/h=0.2$, $c_{fk}/h=0.125$, $d_c/h=1$. The motion of buoys and membrane corresponding to Fig. 6 are depicted in Figs. 11~12, in which large motion of buoys and membranes are apparently related to resonance in performance. The motions of front buoy are apparently small compared to those of rear ones since front one is strongly moored by type 3 at side edge and joint of buoy. The overall shape of sway and joint motion amplitude are quit similar to each other with respect to the various kh and θ. The magnitude of sway and roll motions in front buoys are quite different with those of rear one. The amplitude motion of joints of both buoy $\xi_{joint}=\eta_o=\eta_1+R\eta_3$, however, are similar to each other in magnitude. The motion of buoys is affected by initial tension of membrane for restoring forces or excitations as shown in Eq. (25). Thus the sway and roll motion is strongly coupled with a motion amplitude of the membrane element near joint. In Fig. 11a, the resonance sway motion $\eta_{1f}/A=0.25$ of front buoy at kh=1.3 behaves like skewed curve slightly deviated to higher kh direction as θ is increased. It is reduced to $\eta_{1f}/A=0.1$ at the region of $\theta=85^\circ$ and $kh=3.0$. The rear buoy sway motion at resonance frequency in Fig. 11b, however, keeps same magnitude at the corresponding frequencies and angles. Along the skewed resonance curve in the plain of kh and θ, the increased wave heading does not mitigate the amplitude of rear buoy motion restrained by only joint mooring (mooring type 2).

Finally, Figs. 12a~12b shows the amplitude motions of front and rear membranes. The pattern of motions of front membrane is different with that of rear one except $kh=1.2$. It is mainly due to different design parameters for both systems. In Figs. 12c~12f, the amplitude of membrane motion drastically reduced except at resonance frequencies as θ is increased from 45° to 82°. The amplitudes of rear membrane motions $|\xi_r|/A$ for various wave headings $\theta=0^\circ, 45^\circ, 82^\circ$ seem to be slightly varied as 0.41, 0.37, 0.33. The corresponding peak frequency migrates toward to

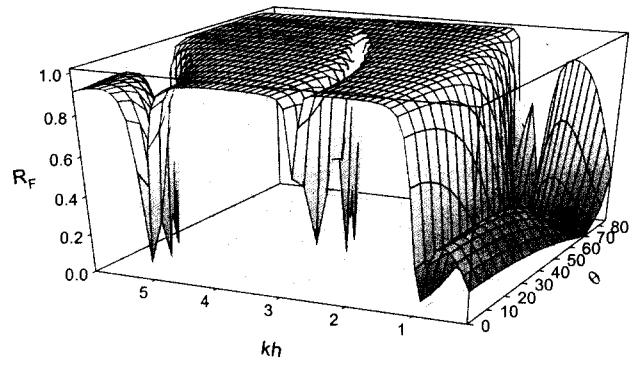

Fig. 7 The reflection coefficient as function kh and θ for $T_i/K_{i1}=0$, $T_i/K_{i2}=0.1$, $t_i/a_i=0.02$, $a_i/h=0.2$, $c_{ik}/h=0.125$, $d_c/h=1$

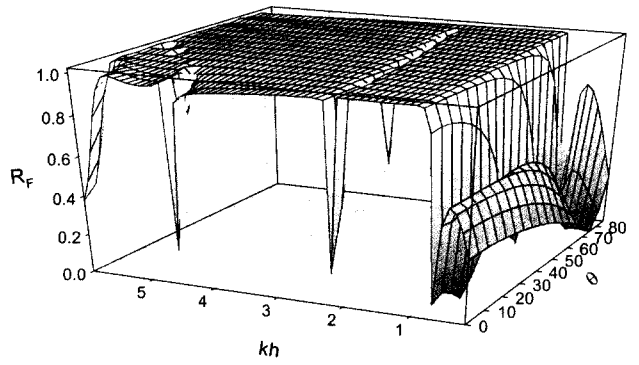

Fig. 8 The reflection coefficient as function kh and θ for $T_i/K_{i1}=0$, $T_i/K_{i2}=0.1$, $t_i/a_i=0.02$, $a_i/h=0.2$, $c_{ik}/h=0.05$, $d_c/h=1$

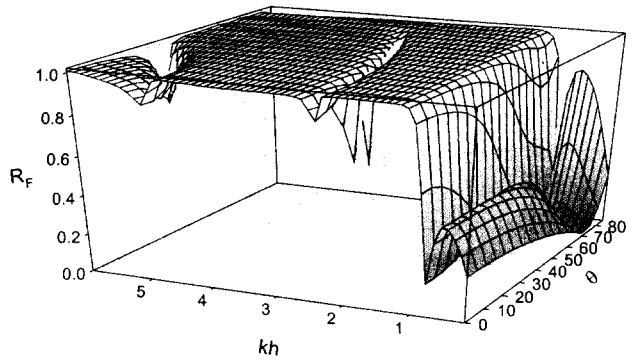

Fig. 9 The reflection coefficient as function kh and θ for $T_i/K_{i1}=0$, $T_i/K_{i2}=0.1$, $t_i/a_i=0.02$, $a_i/h=0.2$, $c_{ff}/h=0.125$, $c_{fb}/h=0.05$, $c_{rf}/h=0.05$, $c_{rb}/h=0.125$, $d_c/h=1$

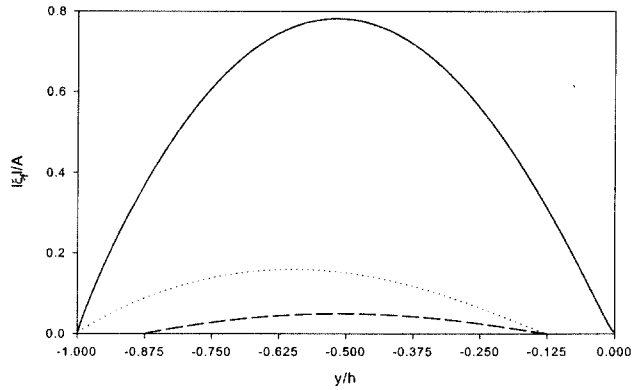

Fig. 10a Front membrane motion as function of vertical coordinate y/h for nondimensional wave number $kh=0.2$, $c_{fk}/h=0$(——), $c_{ff}/h=0.125$ & $c_{fb}/h=0$ (-------), $c_{ff}/h=0.125$ & $c_{fb}/h=0.125$(– – –)

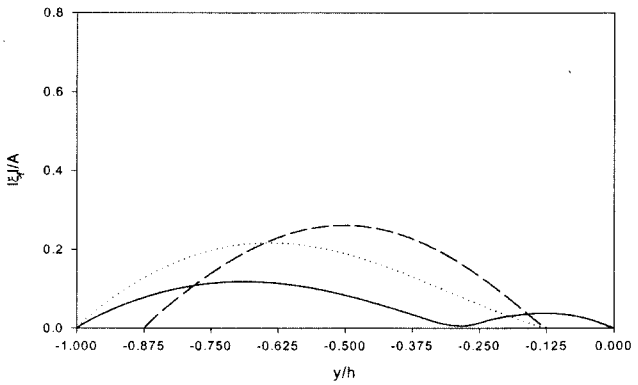

Fig. 10b Front membrane motion as function of vertical coordinate y/h for nondimensional wave number $kh=6$, $c_{fk}/h=0$(——), $c_{ff}/h=0.125$ & $c_{fb}/h=0$(-------), $c_{ff}/h=0.125$ & $c_{fb}/h=0.125$(– – – –)

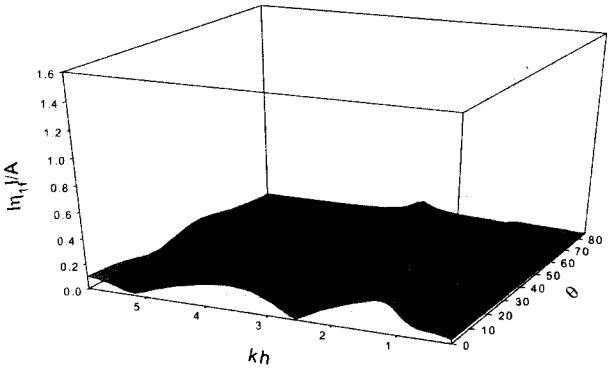

Fig. 11a Sway motion of front cylinder as function kh and θ for $T_f/K_{fj}=0.1$, $T_r/K_{r1}=0$, $T_r/K_{r2}=0.1$, $t_i/a_i=0.02$, $a_i/h=0.2$, $c_{ik}/h=0.125$, $d_c/h=1$

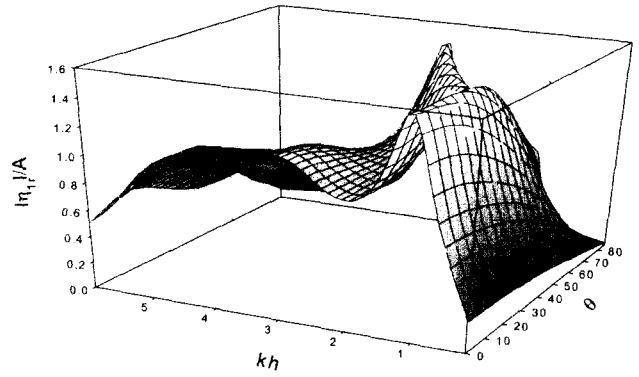

Fig. 11b Sway motion of rear cylinder as function kh and θ for $T_f/K_{fj}=0.1$, $T_r/K_{r1}=0$, $T_r/K_{r2}=0.1$, $t_i/a_i=0.02$, $a_i/h=0.2$, $c_{ik}/h=0.125$, $d_c/h=1$

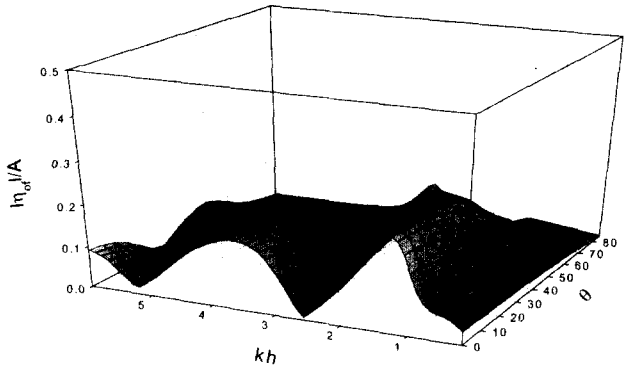

Fig. 11e Joint motion of front cylinder as function kh and θ for $T_f/K_{fj}=0.1$, $T_r/K_{r1}=0$, $T_r/K_{r2}=0.1$, $t_i/a_i=0.02$, $a_i/h=0.2$, $c_{ik}/h=0.125$, $d_c/h=1$

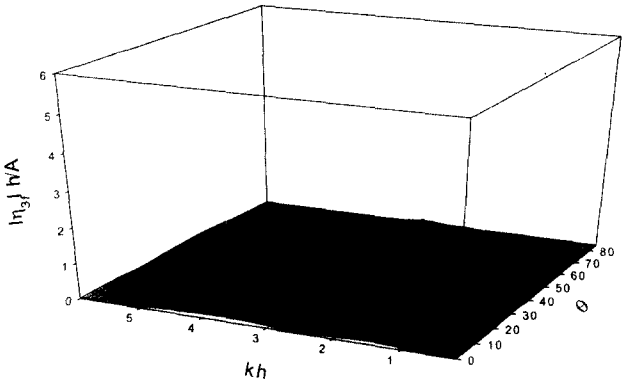

Fig. 11c Roll motion of front cylinder as function kh and θ for $T_f/K_{fj}=0.1$, $T_r/K_{r1}=0$, $T_r/K_{r2}=0.1$, $t_i/a_i=0.02$, $a_i/h=0.2$, $c_{ik}/h=0.125$, $d_c/h=1$

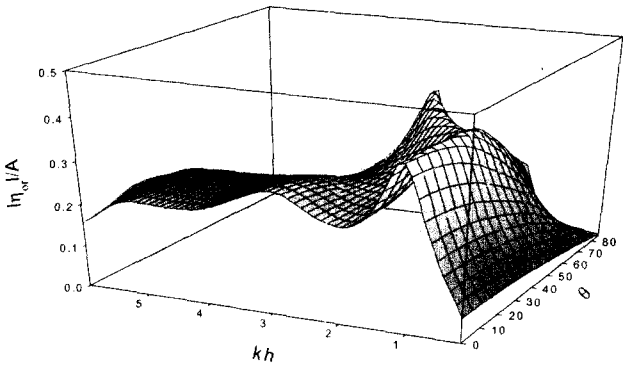

Fig. 11f Joint motion of rear cylinder as function kh and θ for $T_f/K_{fj}=0.1$, $T_r/K_{r1}=0$, $T_r/K_{r2}=0.1$, $t_i/a_i=0.02$, $a_i/h=0.2$, $c_{ik}/h=0.125$, $d_c/h=1$

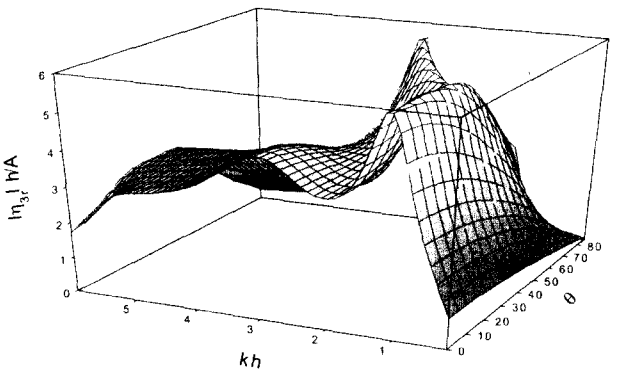

Fig. 11d Roll motion of rear cylinder as function kh and θ for $T_f/K_{fj}=0.1$, $T_r/K_{r1}=0$, $T_r/K_{r2}=0.1$, $t_i/a_i=0.02$, $a_i/h=0.2$, $c_{ik}/h=0.125$, $d_c/h=1$

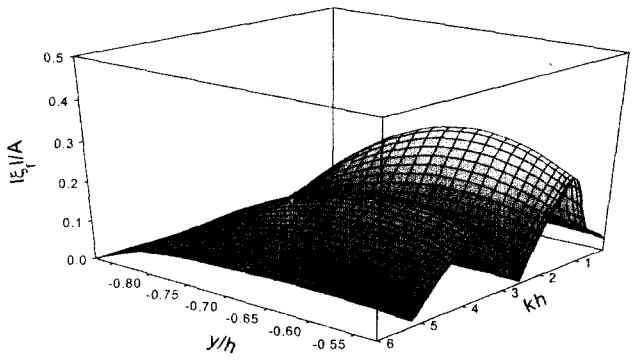

Fig. 12a The motion of front membrane as a function of vertical position y/h and kh for $\theta=0°$, $T_f/K_{fj}=0.1$, $T_r/K_{r1}=0$, $T_r/K_{r2}=0.1$, $t_i/a_i=0.02$, $a_i/h=0.2$, $c_{ik}/h=0.125$, $d_c/h=1$

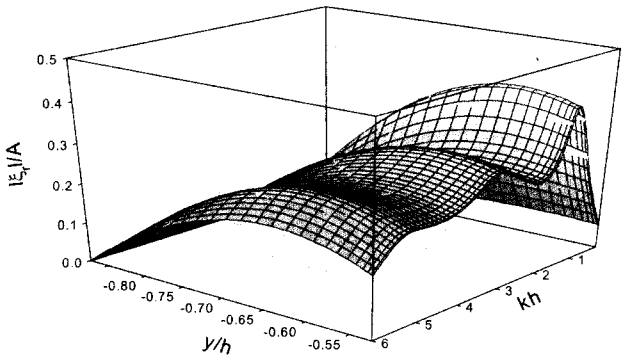

Fig. 12b The motion of rear membrane as a function of vertical position y/h and kh for $\theta=0^\circ$, $T_f/K_{fj}=0.1$, $T_r/K_{r1}=0$, $T_r/K_{r2}=0.1$, $t_i/a_i=0.02$, $a_i/h=0.2$, $c_{ik}/h=0.125$, $d_c/h=1$

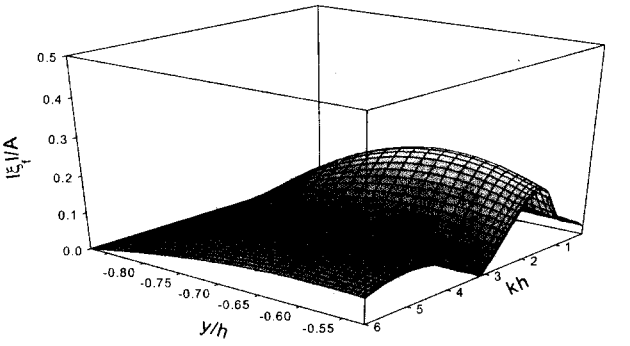

Fig. 12c The motion of front membrane as a function of vertical position y/h and kh for $\theta=45^\circ$, $T_f/K_{fj}=0.1$, $T_r/K_{r1}=0$, $T_r/K_{r2}=0.1$, $t_i/a_i=0.02$, $a_i/h=0.2$, $c_{ik}/h=0.125$, $d_c/h=1$

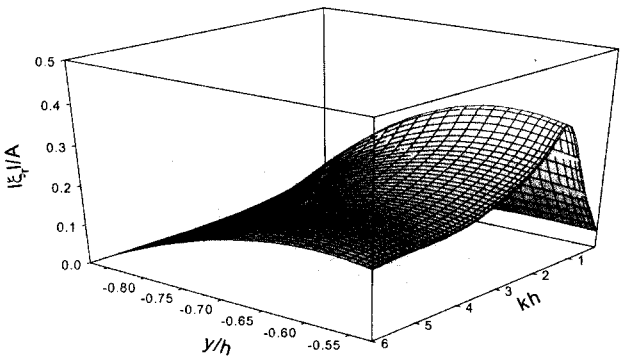

Fig. 12d The motion of rear membrane as a function of vertical position y/h and kh for $\theta=45^\circ$, $T_f/K_{fj}=0.1$, $T_r/K_{r1}=0$, $T_r/K_{r2}=0.1$, $t_i/a_i=0.02$, $a_i/h=0.2$, $c_{ik}/h=0.125$, $d_c/h=1$

high frequency values as $kh=1.18, 1.38, 2.95$. In vicinity of the high wave heading $\theta=82^\circ$ large amplitude of membrane motion at $kh=2.95$ does not affect the performance as shown in Fig. 6. However, smaller amplitude $|\xi_r|/A=1.85$ at $kh=1.48$ suppresses slightly its efficiency. It is interesting to note that the extraordinary large motions of buoy/membrane at resonance frequency heavily in vicinity of lower wave headings suppress the efficiency, but in vicinity of higher wave headings slightly aggravate the performance.

SUMMARY AND CONCLUSIONS

The interaction of oblique incident waves with dual tensioned, inextensible, vertical flexible membranes hinged at some distance from the sea floor and attached to rigid cylindrical submerged buoys at their tops, was solved in the context of two-dimensional

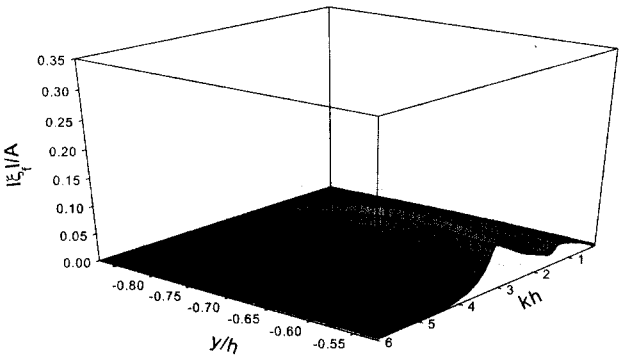

Fig. 12e The motion of front membrane as a function of vertical position y/h and kh for $\theta=82^\circ$, $T_f/K_{fj}=0.1$, $T_r/K_{r1}=0$, $T_r/K_{r2}=0.1$, $t_i/a_i=0.02$, $a_i/h=0.2$, $c_{ik}/h=0.125$, $d_c/h=1$

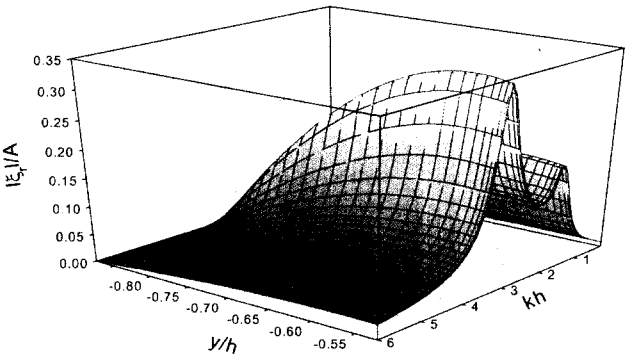

Fig. 12f The motion of rear membrane as a function of vertical position y/h and kh for $\theta=82^\circ$, $T_f/K_{fj}=0.1$, $T_r/K_{r1}=0$, $T_r/K_{r2}=0.1$, $t_i/a_i=0.02$, $a_i/h=0.2$, $c_{ik}/h=0.125$, $d_c/h=1$

linear wave-body interaction theory. For numerical approaches to more practical and eco-friendly buoy-membrane systems, a boundary element program was developed based on a discrete-membrane dynamic model and simple-source distribution over the entire fluid boundaries. A three-domain BEM was employed since the membrane is infinitely thin. The solutions of each domain were matched at the respective membrane surfaces. Membrane motions and velocity potentials were solved simultaneously because the body-boundary condition on the membrane is not known in advance, as other hydro elastic problems. The accuracy and convergence of the developed computer program are checked using the energy-conservation formula and convergence test.

Using the developed computer program, the performance of fully submerged dual systems in oblique waves was tested with various breakwater design parameters, and wave conditions. From these examples, it is shown that the use of the submerged dual flexible membranes can significantly increase the overall wave blocking efficiency in normal and oblique incident waves except long waves. Allowing motion of buoys, the mutual cancellation effect of incident waves and scattered waves significantly enhance the performance of breakwaters. Using a properly devised asymmetric system, which can complement each other, we can further enhance the efficiency for $T_i/K_{i1}=0$, $T_i/K_{i2}=0.1$, $t_i/a_i=0.02$, $a_i/h=0.2$, $c_{ff}/h=0.125$, $c_{fb}/h=0.05$, $c_{rf}/h=0.05$, $c_{rb}/h=0.125$, $d_c/h=1$. In most cases, mooring type, gaps, and size of buoy for sufficiently large membrane tension needs to be provided to guarantee high performance over a wide range of wave frequencies.

ACKNOWLEDGMENT

This research was sponsored by the Korea Institute of Construction Technology (KICT) Research Center Program, Grant Number R&F/00-24-01.

REFERENCES

Amal C. Phadke, Kwok Fai Cheung (2001). "Resonance and response of fluid-filled membrane in gravity waves", J. Applied Ocean Research, Vol. 23, pp 15~28.

Aoki, S., Liu, H., & Sawaragi, T. (1994). "Wave transformation and wave forces on submerged vertical membrane", Proc. Intl. Symp. Waves - Physical and Numerical Modeling, Vancouver, pp 1287~1296

Cho, I.H. & Kim, M.H. (2000). "Interactions of Horizontal Porous Flexible Membrane with Waves" ASCE J. of Waterway, Port, Coastal & Ocean Engineering, Vol. 126, No. 5, pp 245~253.

Cho, I.H. & Kee, S.T & Kim, M.H. (1998). "The Performance of Dual Flexible Membrane Wave Barrier in Oblique Sea", ASCE J. of Waterway, Port, Coastal & Ocean Engineering, Jan./Feb. 1998 Vol. 124, No. 1, pp 21~30

Cho, I.H. & Kee, S.T. & Kim, M.H. (1997). "The Performance of Dual Flexible Membrane Wave Barrier in Oblique Incident Waves" J. of Applied Ocean Research, Jun./Aug. 1997. Vol. 19, No. 3-4, pp 171~182

Kee, S.T. & Kim, M.H. (1997). "Flexible membrane wave barrier. Part 2. Floating/submerged buoy-membrane system", ASCE J. of Waterway, Port, Coastal & Ocean Engineering, Vol. 123, No. 2, pp 82~90.

Kim, M.H. & Kee, S.T. (1996). "Flexible membrane wave barrier. Part 1. Analytic and numerical solutions", ASCE J. of Waterway, Port, Coastal & Ocean Engineering, Vol. 122, No. 1, pp 46~53.

Patel, Minoo H.(1989). Dynamics of offshore structures. Butterworths, Boston.

Thompson, G.O., Sollitt, C.K., McDougal, W.G. & Bender W.R. (1992). "Flexible membrane wave barrier", ASCE Conf. Ocean V, College Station, pp 129~148.

Williams, A.N. (1996). "Floating membrane breakwater", J. of Offshore Mechanics & Arctic Engr., Vol. 118, pp 46~51.

2001년 1월 28일 원고 접수
2001년 3월 25일 수정본 채택